In vivo depth-resolved birefringence measurements of the human retinal nerve fiber layer by polarization-sensitive optical coherence tomography

Barry Cense

Wellman Laboratories of Photomedicine, Harvard Medical School, Massachusetts General Hospital, BAR 714, Boston, Massachusetts 02114

Teresa C. Chen

Massachusetts Eye and Ear Infirmary and Harvard Medical School, 243 Charles Street, Boston, Massachusetts 02114

B. Hyle Park, Mark C. Pierce, and Johannes F. de Boer

Wellman Laboratories of Photomedicine, Harvard Medical School, Massachusetts General Hospital, BAR 714, Boston, Massachusetts 02114

Received April 3, 2002

To our knowledge, this is the first demonstration of *in vivo* depth-resolved birefringence measurements of the human retinal nerve fiber layer (RNFL) by use of polarization-sensitive optical coherence tomography (PS-OCT). Because glaucoma causes nerve fiber layer damage, which may cause loss of retinal birefringence, PS-OCT is a potentially useful technique for the early detection of glaucoma. We built a fiber-based PS-OCT setup that produces quasi-real-time images of the human retina *in vivo*. Preliminary measurements of a healthy volunteer showed that the double-pass phase retardation per unit depth of the RNFL near the optic nerve head is $39 \pm 6^{\circ}/100\ \mu$m. © 2002 Optical Society of America

OCIS codes: 110.7050, 170.4460, 170.4500, 260.1440.

Glaucoma is the world's second leading cause of blindness. Glaucoma causes damage to the retinal ganglion cells, resulting in thinning of the retinal nerve fiber layer (RNFL). When glaucoma is detected at an early stage, further loss of vision can be prevented by medication or surgery. Currently, there is no direct method that can measure the health and function of the RNFL. The visual field test is the current standard method of subjectively detecting loss of peripheral vision from glaucoma. However, measurements show that as much as 40% of the nerves are irreversibly damaged before a loss of peripheral vision occurs.[1] With optical coherence tomography (OCT), cross-sectional structural images of the retina can be made *in vivo*, permitting the determination of the RNFL thickness.[2,3] From light reflected from the retina, scanning laser polarimetry can measure changes in polarization state, which are attributed to the birefringence of the RNFL.[4] Polarization-sensitive OCT (PS-OCT) combines the depth resolution of OCT with the polarization sensitivity of scanning laser polarimetry to image the depth-resolved optical birefringence of biological tissue.[5–8] *Ex vivo* measurements of primate and enucleated rabbit eyes demonstrated birefringence in the RNFL and showed good correlation between thicknesses determined with PS-OCT and with histology.[9,10] Measurement of the RNFL's optical birefringence will enhance specificity in determining its thickness in structural OCT images. Although this is now a speculation, it is believed that a decrease in birefringence could be an early sign of glaucomatous atrophy of the RNFL.

To measure RNFL birefringence in human subjects *in vivo*, we built a fiber-based PS-OCT setup that produces quasi-real-time images of the retina. The experimental configuration (Fig. 1) was based on previous fiber-based OCT designs.[7,8] A superluminescent diode generated a broadband spectrum with a power of 0.8 mW (before polarization) and with a FWHM bandwidth of 45 nm centered at 830 nm, giving a measured coherence length in free space of $7 \pm 1\ \mu$m (FWHM). In the retina, the axial resolution is equal to $5.1 \pm 0.8\ \mu$m, assuming a refractive index of 1.38. In previous open-air PS-OCT systems

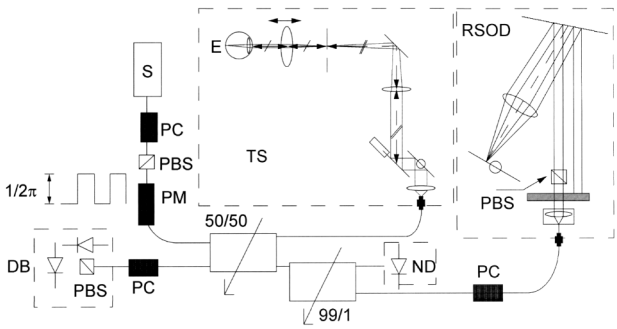

Fig. 1. Schematic of the experimental setup. Light emitted by the source (S) is polarized with one of three polarizing beam splitters (PBSs) and modulated with a polarization modulator (PM) before it enters the 50/50 splitter. Balanced detection is implemented by means of a 99/1 splitter and a noise detector (ND). The reference arm is a rapid scanning optical delay line (RSOD). The sample arm contains a telecentric scanner (TS), which pivots a beam through the eye's pupil (E) by means of a set of galvo mirrors and two lenses. In the detector bench (DB), light is split into its two orthogonal components by a polarizing beam splitter and detected by two detectors. Polarization controllers (PCs) permit tuning of the polarization state at various locations in the setup.

0146-9592/02/181610-03$15.00/0

the tissue was usually probed with circularly polarized light.[5,6] In a fiber-based PS-OCT system it is difficult to maintain a circular polarization state at the sample surface.[7] This problem was overcome by a relative measurement method in which the tissue was probed with four different polarization states.[7,8] Here we have used only two polarization states, which were 90° apart on the Poincaré sphere and were generated by means of a piezo-driven polarization modulator in the source arm. A 50/50 fiber-based splitter divided the light between sample and reference arms. The sample arm consisted of a telecentric XY retina scanner and a headrest from a standard slit lamp. Because aberrations are incurred in the cornea and the lens, optimal spot size (and therefore maximum retinal reflection) is obtained when the beam has a width of approximately 2–3 mm at the pupil plane.[11] A linear scan that covers a length of 1.5 mm in 2 s on the retina was used. The power incident upon the eye was 136 μW, well below the ANSI standard limit.[12] The reference arm of our system consisted of a rapid scanning optical delay line[13] (RSOD) with a polarizing beam splitter to ensure that light in the RSOD was always in the same linear state, regardless of changes in the polarization state in the fiber before the RSOD. A polarization controller before the RSOD was aligned such that the power reflected from the RSOD was constant for both input polarization states. We matched the dispersion in the sample and reference arms by adjusting the grating to the lens distance in the delay line. The delay line's scanning mirror was positioned off axis and driven by a triangular waveform with a frequency of 128 Hz, synchronized with the polarization modulator, which was driven by a block wave of the same frequency. The carrier signal was at approximately 300 kHz. During one 2-s B scan, 512 A lines with a length of 8192 samples were acquired. The detection arm consisted of a polarization controller and a polarizing beam splitter that split the light into two orthogonal components before detection by two silicon detectors. To compensate for excessive source noise near 300 kHz, we implemented a method for balanced detection by sending 1% of the reference arm's power to a reference noise detector. We removed source noise by subtracting the reference noise signal from the two orthogonal polarization signals. These three signals were digitized with a 12-bit, 2.5-MHz analog-to-digital conversion board and immediately stored to hard disk. All experiments were performed under a protocol approved by the institutional review boards of both the Massachusetts Eye and Ear Infirmary and the Massachusetts General Hospital. Experiments were performed on a healthy 37-year-old adult who had given informed consent. Before to the measurements, the volunteer's right eye was dilated with a solution of phenylephrine hydrochloride 5.0% and tropicamide 0.8%.

Figure 2 presents an intensity image that was recorded in an area near the optic nerve head. Structural features of the layers in the retina are evident. The dynamic range of the gray-scaled B scan is ~23 dB. The intensity images were not corrected for motion artifacts. By demodulation with respect to the carrier frequency, the number of samples within one A line was reduced from 8192 to 1024 Stokes vectors I, Q, U, and V, as described earlier.[6–8] An intensity image therefore consisted of 512 A lines, each showing 1024 intensity pixels I, gray-scale encoded on a logarithmic scale. We used two adjacent A lines, created with two different input polarization states, to calculate one double-pass phase retardation (DPPR) A line. In the DPPR calculation we achieved a considerable reduction of speckle noise by averaging the Stokes parameters of 32 adjacent A lines with the same input polarization state. The surface Stokes vector was calculated 10 μm below the surface edge, which was determined from the I Stokes parameter by a threshold function preceded by a 3×3 median filter. To determine the DPPR of the RNFL we compared Stokes vectors at the RNFL's surface with Stokes vectors at lower depths to determine DPPR and optic axis orientation.[6–8] Figure 3 shows the evolution of the two incident Stokes states over the surface of the Poincaré sphere with increasing depth of tissue for the region of 64 A lines delineated in Fig. 2. The rotation of both states over an arc about a single axis explicitly demonstrates birefringence with a single optic axis, as expected for the regularly oriented fibers in the RNFL. The angle of rotation, starting at the places marked X, corresponds to accumulated DPPR as a function of depth. The angle between two equidistant Stokes vectors was approximately 90°.

Corneal birefringence changes the incident polarization state unpredictably.[14] Because the RNFL surface is used as a reference in the DPPR calculation, our method is not influenced by corneal birefringence.

We analyzed three consecutive images to quantify the birefringence of the RNFL. In these images the RNFL was divided into 8 regions, each with 64 A lines. The DPPR as a function of depth for each region of 64 A lines was calculated. Data points that were considered to originate from the RNFL were

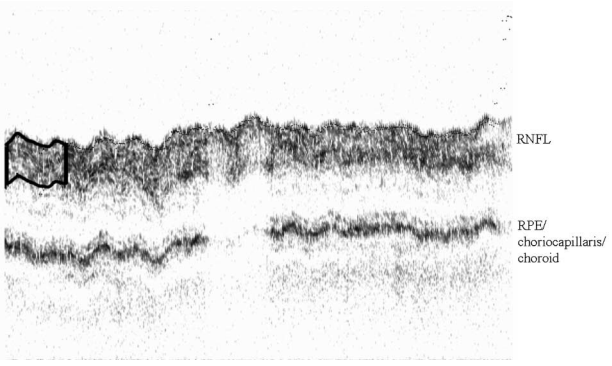

Fig. 2. Area near the optic nerve head. The image measures width × depth = 1024 × 512 pixels = 1 mm × 1.5 mm. The dark top layer is the RNFL, with a thickness of ~100 μm. The loss of signal in the deeper layers in the center of the image is probably caused by the presence of two blood vessels in the RNFL. Double-pass phase-retardation calculations were performed on regions of 64 averaged A lines exemplified by the black-bordered area in the upper left corner.

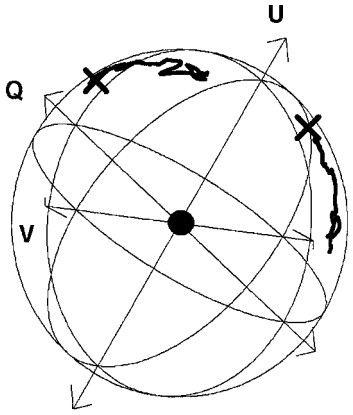

Fig. 3. Evolution of the Stokes vectors with depth, from data averaged over 64 A lines. The Poincaré sphere is oriented such that the axis of rotation is pointing out of the plane of the drawing. The two thick lines show the change in Stokes vectors over a distance of 100 μm in the RNFL, and X's indicate the surface Stokes states. The DPPR is derived from the angle of rotation about the optic axis, starting with the Stokes vector that belongs to the surface and finishing with the vector that belongs to a certain depth.

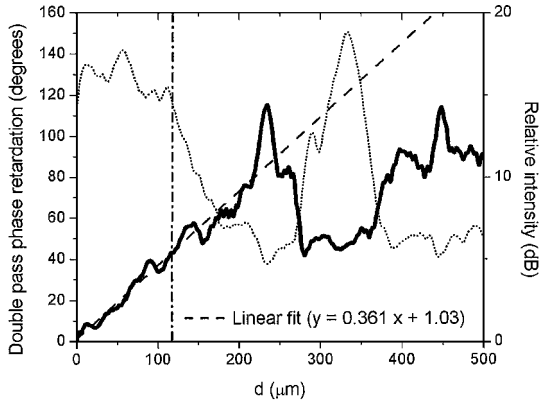

Fig. 4. DPPR as a function of depth, with the data from Figs. 2 and 3. Solid curve, DPPR; dotted curve, reflected intensity; dashed curve, least-squares linear fit to DPPR data over a region considered to belong to the RNFL. The vertical dashed–dotted line represents the estimated RNFL boundary.

fitted with a linear least-squares fit, with the slope yielding the reported DPPR. We used the corresponding intensity graph to determine the boundaries of the RNFL. As an example, Fig. 4 shows the DPPR, the reflected intensity, and a linear fit to the double-pass phase retardation, which corresponds to the delineated area in Fig. 2 and the data in Fig. 3. In the region where the reflected intensity drops significantly (at 120–280 μm), the DPPR measurement is unreliable and drifts to 115°.[8] In the region of strong reflectance from the retinal pigment epithelium–choroid (300–360 μm), a DPPR value that corresponds to the bottom of the RNFL is measured, indicating an absence of birefringent structures between the RNFL and the retrieval pigment epithelium-choroid.

The DPPR values of all regions of the three images were averaged, and the standard deviation was calculated. Regions with visible blood vessels (as seen, for example, in the center of Fig. 2) were excluded, because the absence of birefringence in blood vessels distorted the DPPR measurement in nerve tissue. Averaging the results of 20 blocks of 64 A lines yielded a DPPR per unit depth of 39 ± 6°/100 μm and a thickness of the RNFL of 110 ± 20 μm. Ducros *et al.* measured the DPPR at a wavelength of 859 nm in the RNFLs of primates.[10] They found a typical value of 29°/100 μm, which is in the same range as our measured values.

In conclusion, PS-OCT is a modality suitable for *in vivo* depth-resolved birefringence measurements of the human retina. Preliminary measurements of one volunteer showed a DPPR in the RNFL near the optic nerve head of 39 ± 6°/100 μm.

Research grants from the National Eye Institute (1R 24 EY 12877) and the Whitaker Foundation (26083) for the support of this research are gratefully acknowledged by the authors. The first- and last-named authors' e-mail addresses are bcense@helix.mgh.harvard.edu and deboer@helix.mgh.harvard.edu.

References

1. H. A. Quigley, E. M. Addicks, and W. R. Green, Arch. Ophthalmol. **100,** 135 (1982).
2. J. S. Schuman, M. R. Hee, C. A. Puliafito, C. Wong, T. Pedut-Kloizman, C. P. Lin, E. Hertzmark, J. A. Izatt, E. A. Swanson, and J. G. Fujimoto, Arch. Ophthalmol. **113,** 586 (1995).
3. W. Drexler, U. Morgner, R. K. Ghanta, F. X. Kärtner, J. S. Schuman, and J. G. Fujimoto, Nature Med. **7,** 502 (2001).
4. R. N. Weinreb, A. W. Dreher, A. Coleman, H. Quigley, B. Shaw, and K. Reiter, Arch. Ophthalmol. **108,** 557 (1990).
5. J. F. de Boer, T. E. Milner, M. J. C. van Gemert, and J. S. Nelson, Opt. Lett. **22,** 934 (1997).
6. J. F. de Boer, T. E. Milner, and J. S. Nelson, Opt. Lett. **24,** 300 (1999).
7. C. E. Saxer, J. F. de Boer, B. H. Park, Y. Zhao, Z. Chen, and J. S. Nelson, Opt. Lett. **25,** 1355 (2000).
8. B. H. Park, C. E. Saxer, S. M. Srinivas, J. S. Nelson, and J. F. de Boer, J. Biomed. Opt. **6,** 474 (2001).
9. M. G. Ducros, J. F. de Boer, H. E. Huang, L. C. Chao, Z. Chen, J. S. Nelson, T. E. Milner, and H. G. Rylander, IEEE J. Sel. Top. Quantum Electron. **5,** 1159 (1999).
10. M. G. Ducros, J. D. Marsack, H. G. Rylander, S. L. Thomsen, and T. E. Milner, J. Opt. Soc. Am. A **18,** 2945 (2001).
11. F. W. Campbell and D. G. Green, J. Physiol. **181,** 576 (1965).
12. American National Standards Institute, "Safe use of lasers," standard ANSI Z136.1 (Laser Institute of America, New York, 1993).
13. G. J. Tearney, B. E. Bouma, and J. G. Fujimoto, Opt. Lett. **22,** 1811 (1997).
14. D. S. Greenfield, R. W. Knighton, and X. Huang, Am. J. Ophthalmol. **129,** 715 (2000).